Matter

CellPress

Article

Immune-Instructive Polymers Control Macrophage Phenotype and Modulate the Foreign Body Response *In Vivo*

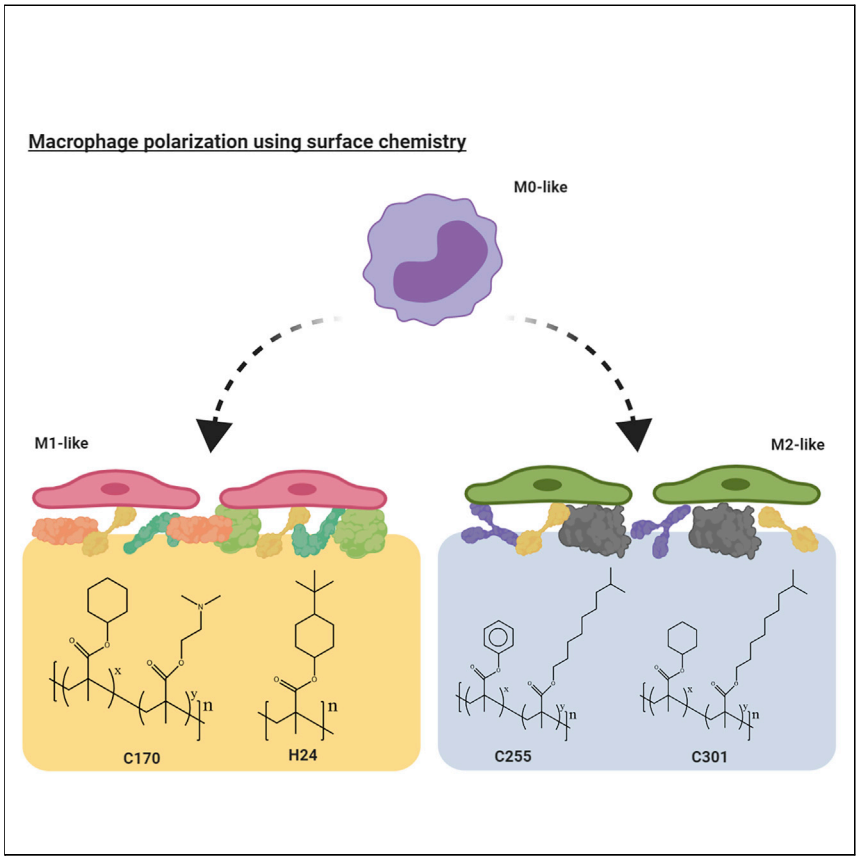

Implantation of medical devices can result in inflammation. A large library of polymers is screened, and a selection found to promote macrophage differentiation towards pro- or anti-inflammatory phenotypes. The bioinstructive properties of these materials are validated within a rodent model. By identifying novel materials with immune-instructive properties, the relationship between material-immune cell interactions could be investigated, and this offers exciting possibilities to design novel bioinstructive materials that can be used for numerous clinical applications including medical implants.

Benchmark
First qualification/assessment of material properties and/or performance

Hassan M. Rostam, Leanne E. Fisher, Andrew L. Hook, ..., David A. Winkler, Morgan R. Alexander, Amir M. Ghaemmaghami

morgan.alexander@nottingham.ac.uk (M.R.A.)
amir.ghaemmaghami@nottingham.ac.uk (A.M.G.)

HIGHLIGHTS

In vitro screening identifies polymers with potent immune-modulatory properties

Polymers were able to modulate the foreign body response within a murine model

Polymer structure-cell response relationships were modeled using machine learning

Rostam et al., Matter *2*, 1–18
June 3, 2020
https://doi.org/10.1016/j.matt.2020.03.018

Please cite this article in press as: Rostam et al., Immune-Instructive Polymers Control Macrophage Phenotype and Modulate the Foreign Body Response *In Vivo*, Matter (2020), https://doi.org/10.1016/j.matt.2020.03.018

Matter

CellPress

Article

Immune-Instructive Polymers Control Macrophage Phenotype and Modulate the Foreign Body Response *In Vivo*

Hassan M. Rostam,[1,10,11] Leanne E. Fisher,[1,11] Andrew L. Hook,[2] Laurence Burroughs,[2] Jeni C. Luckett,[3] Grazziela P. Figueredo,[4] Chidimma Mbadugha,[1] Alvin C.K. Teo,[2] Arsalan Latif,[1] Lisa Kämmerling,[1] Mitchell Day,[1] Karen Lawler,[1] David Barrett,[2] Somaia Elsheikh,[5] Mohammad Ilyas,[6] David A. Winkler,[2,7,8,9] Morgan R. Alexander,[2,*] and Amir M. Ghaemmaghami[1,12,*]

SUMMARY

Implanted medical devices often elicit adverse foreign body responses whereby macrophages play a central role. Here, we identify simple polymers that instruct different immunological responses by modulating macrophage attachment and polarization to pro-inflammatory (M1-like) or anti-inflammatory (M2-like) phenotypes. These immune-instructive polymers were discovered using *in vitro* high-throughput polymer microarray screening of diverse (meth)acrylate and (meth)acrylamide libraries. The bioinstructive polymer function is validated *in vivo* within a murine foreign body model. Differential tissue response from polymers coated on silicone tubing is consistent with *in vitro* macrophage pro- and anti-inflammatory responses. Polymer structure-cell response relationships are modeled using machine learning to reveal molecular descriptors useful for describing immune-instructive polymers. Analysis of the protein layer adsorbed to polymers from media suggests that thicker layers may relate to M1-like phenotype whereas the reverse relates to M2-like response. Such simple polymers are readily translatable into immune-instructive biomaterials for application in the medical device and regenerative medicine fields.

INTRODUCTION

Implantable medical devices are limited by the foreign body response to the biomaterials from which they are made.[1–3] This response can lead to chronic inflammation, tissue damage, and fibrosis, resulting in device rejection and failure.[4,5] Macrophages are equipped with a plethora of receptors that enable them to monitor subtle changes in their microenvironment. In response to such changes they acquire a spectrum of functional phenotypes with pro- and anti-inflammatory abilities.[6–9] While both pro- and anti-inflammatory cells are essential for an efficient immune response and orderly resolution of post-infection inflammation or tissue damage, sustained activation of either subset is undesirable. The responsiveness of macrophages to environmental changes, together with their functional plasticity, provides opportunities for developing "immune-instructive" niches where the macrophage phenotype can be controlled by changing the chemical and physical attributes of materials they contact.[10] Indeed, previous studies have shown that changes in the physical and chemical properties of biomaterials can influence macrophage adhesion and polarization status.[3,5,11] Here, we investigated the application of

Progress and Potential

This study explores the hypothesis that simple polymer chemistries can be used to modulate the phenotype of human immune cells. Unbiased high-throughput screening of a large library of polymer chemistries is undertaken, identifying materials able to instruct macrophage attachment and polarization to pro- or anti-inflammatory phenotypes. The bioinstructive polymer function is validated by a murine model in which modulation of the foreign body response is shown. Polymer structure-cell response relationships modeled using machine learning reveal molecular descriptors useful for interpreting the immune-instructive polymers, highlighting the potential to undertake "immune-instructive" rational design. Identifying new polymers with immune-modulatory properties and elucidating the molecular mechanisms involved offer exciting possibilities to create novel bioinstructive materials with numerous clinical applications from implants and vaccine adjuvants to regenerative medicine and drug delivery.

high-throughput biomaterial microarray screening methods to discover immune-instructive materials. Previous work has highlighted the potential of high-throughput screening of combinatorial polymer libraries to discover polymers that could not have been predicted by theory to achieve low bacterial biofilm formation or pluripotent stem cell expansion and differentiation.[12–16] We hypothesized that chemically diverse libraries of simple polymers could also be used to identify materials with immune-modulatory properties, in particular the ability to alter macrophage phenotype. To examine this hypothesis, we initially screened a library of homopolymers consisting of 141 meth(acrylate) and meth(acrylamide) monomers for their ability to induce the differentiation of human monocytes to distinct macrophage phenotypes using fluorescent labels of surface markers to categorize cells into M1-like or M2-like phenotypes. Homopolymers of interest were selected from this screen to produce a second-generation polymer library by co-polymerizing the monomers. A 400-member co-polymer array was produced, which was screened for "hit" materials selected based on cell attachment and their ability to induce M1- and M2-like phenotypes in macrophages. These were then scaled up and used in a series of *in vitro* and *in vivo* experiments to assess their ability to modulate macrophage phenotype and response to an implanted foreign body (Figure 1).

RESULTS AND DISCUSSION

High-Throughput Polymer Chemistry Screening Identifies Immunomodulatory Materials

Using a high-throughput screening strategy, we investigated the effect of a combinatorial library of polymers on macrophage attachment, morphology, and phenotype over a 6-day culture.[17–19] Monocytes from three different healthy donors were cultured on the first-generation array composed of three replicates of 141 unique (meth)acrylate and (meth)acrylamide homopolymers intended to screen a broad range of chemistries (Table S1). Cell attachment to a biomaterial surface is a prerequisite to study cell behavior and cell-instructive properties. It is also vital in order to stimulate cell activation and polarization in response to the differing polymers. Since a high-throughput screening approach was used to study the ability of hundreds of polymers to polarize macrophages, there is a need for high-throughput automated image-based analysis, and to do this cell attachment and surface marker expression, as a surrogate for phenotyping, are well suited to this kind of analysis.[18,20] The proportion of pro-inflammatory M1-like macrophages was quantified using expression of calprotectin and anti-inflammatory M2-like phenotypes using mannose receptor (MR) expression, first establishing reference fluorescence measurements in cytokine polarized M1 (interferon-γ [IFN-γ] 20 ng/mL + granulocyte macrophage colony-stimulating factor [GM-CSF] 50 ng/mL) or M2-like macrophages (interleukin-4 [IL-4] 20 ng/mL + M-CSF 50 ng/mL) on glass (Figure S1).

The average M2/M1 cell number ratio (from three spots), using cells from three different donors, was calculated for each polymer to identify "hit" materials with the ability to induce M1-like or M2-like differentiation (Figures 2A and 2B). The homopolymer H47: poly-*N*-[tris(hydroxymethyl)methyl] acrylamide (Figure 2C) was most effective in polarizing macrophages toward the M2-like phenotype, with an M2/M1 cell number ratio of nearly 7, but the total cell number average was relatively low (Figure 2B). Two other polymers with high M2/M1 cell number ratios were H37: poly(methacrylamide) (Figure 2D) and H9: poly(tridecafluorooctyl acrylate) with M2/M1 cell number ratio of 4.5 and 3.5, respectively, again with relatively low total cell number average. There were numerous polymers with M2/M1 cell number ratios close to 1, suggesting either evenly split M1- and M2-like populations

[1]School of Life Sciences, University of Nottingham, Nottingham NG7 2RD, UK

[2]School of Pharmacy, University of Nottingham, Nottingham NG7 2RD, UK

[3]Faculty of Medicine and Health Sciences, University of Nottingham, Nottingham NG7 2RD, UK

[4]School of Computer Science, University of Nottingham, Nottingham NG8 1BB, UK

[5]Department of Cellular Pathology, Queens Medical Centre, Nottingham NG7 2UH, UK

[6]Department of Histopathology, Queens Medical Centre, Nottingham NG7 2UH, UK

[7]Monash Institute of Pharmaceutical Sciences, Monash University, Clayton, VIC 3052, Australia

[8]La Trobe Institute for Molecular Science, La Trobe University, Bundoora, VIC 3084, Australia

[9]CSIRO Manufacturing, Clayton, VIC 3168, Australia

[10]Present address: Department of Biology, University of Garmian, Kalar, Kurdistan Region, Iraq

[11]These authors contributed equally

[12]Lead Contact

*Correspondence: morgan.alexander@nottingham.ac.uk (M.R.A.), amir.ghaemmaghami@nottingham.ac.uk (A.M.G.)

https://doi.org/10.1016/j.matt.2020.03.018

Please cite this article in press as: Rostam et al., Immune-Instructive Polymers Control Macrophage Phenotype and Modulate the Foreign Body Response *In Vivo*, Matter (2020), https://doi.org/10.1016/j.matt.2020.03.018

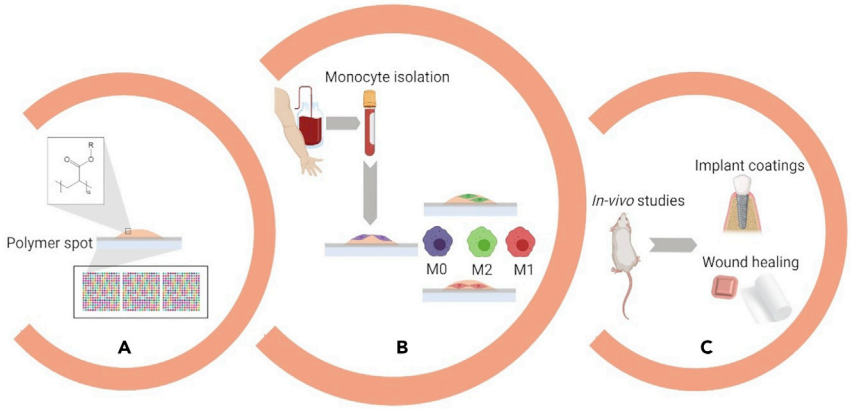

Figure 1. Schematic of the High-Throughput Screening Approach Used to Identify Hit Polymers that Drive Macrophage Phenotype toward a Pro- or Anti-inflammatory Status, *In Vitro* and *In Vivo*

(A and B) (A) High-throughput printing of polymer arrays with different surface chemistries. (B) Monocyte isolation from human buffy coats and seeding onto polymer arrays for 6 days followed by macrophage phenotype assessment determined using a pro-inflammatory (M1) fluorescent marker in red (calprotectin) and an anti-inflammatory (M2) fluorescent marker in green (mannose receptor). (C) A selection of polymers that had high macrophage attachment and polarization ability *in vitro* were coated onto catheter segments and inserted subcutaneously into an *in vivo* mouse model and assessed for their foreign body response. Example application of how polymer coatings could be used to encourage healing in dental and wound applications. Figure created with BioRender.

or naive macrophage (M0) domination (cells stained equally with both markers), e.g., H132: poly(benzyl acrylate). However, H126: poly(isobutyl acrylate) (Figure 2E), H98: poly(hydroxypropyl acrylate) (Figure 2F), and H135: poly(ethylene glycol phenyl ether methacrylate) were the most effective at polarizing cells toward the M1 phenotype with M2/M1cell number ratios of 0.22, 0.41, and 0.42, respectively. The total cell number on each polymer varied across the library by over an order of magnitude from 9.8 $\pm$ 3.9 cells observed on H39: poly(tridecafluorooctyl methacrylate) (Figure 2I) to 230 $\pm$ 65 cells observed on H42: poly(cyclohexyl methacrylate) (Figure 2H). Since these cells do not proliferate, the observed differences in cell number indicate differential cell attachment.[21] A number of homopolymers showed high levels of cell adhesion (H133, H90, H103, H21, H94, H24, H69, H96, H92, and H33) (Figure 2G), with average cell attachment numbers of 209 $\pm$ 48, 197 $\pm$ 69, 171 $\pm$ 32, 169 $\pm$ 18, 168 $\pm$ 33, 151 $\pm$ 120, 147 $\pm$ 8.2, 137 $\pm$ 53, 132 $\pm$ 39, and 127 $\pm$ 25 cells, respectively.

To investigate whether homopolymers inducing macrophage polarization could be combined with those promoting high cell attachment, we used co-polymerization to form a second-generation combinatorial polymer library. For this we selected the top ten homopolymers close to the M2-like cytokine polarized threshold (3.8 $\pm$ 0.6) or the M1-like cytokine polarized threshold (0.4 $\pm$ 0.05) together with ten homopolymers showing the highest cell attachment (Table S2) to create a combinatorial library of 400 co-polymers (Table S3). Using the same procedure as for the first-generation array, purified monocytes were incubated on co-polymer arrays with each individual adhered cell categorized as M1-like or M2-like after 6 days (see Supplemental Experimental Procedures); the ratio is plotted against the number of adherent cells in Figure 3A. Differences between homopolymer and co-polymer threshold ratios are due to the inter-individual variation between cells retrieved from different donors.

Please cite this article in press as: Rostam et al., Immune-Instructive Polymers Control Macrophage Phenotype and Modulate the Foreign Body Response *In Vivo*, Matter (2020), https://doi.org/10.1016/j.matt.2020.03.018

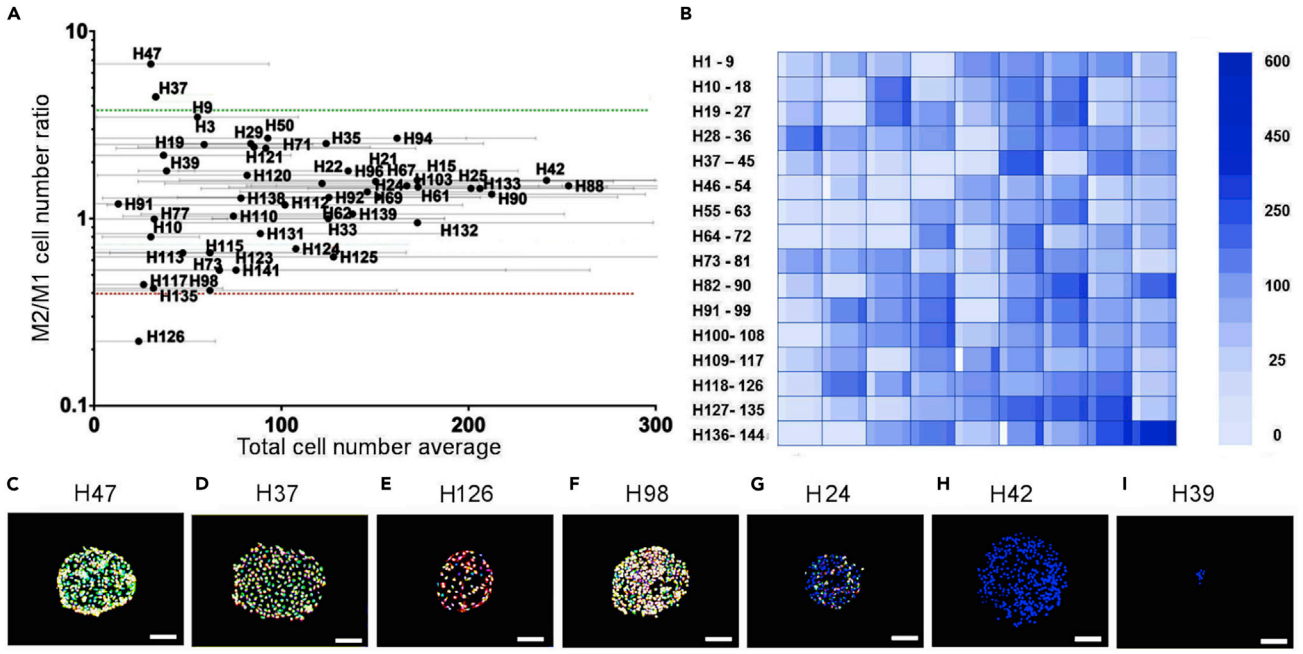

Figure 2. Macrophage Surface Phenotype and Adherence on Homopolymer Arrays

(A) Scatterplot showing M2/M1 cell number ratio for three biological samples. Homopolymers with M2/M1 cell number ratios above the upper green dashed line highlight M2-like homopolymer hits (3.8 ± 0.6) and those below the lower red dashed line (0.4 ± 0.05) show polymers that induced M1-like polarization to a greater extent than in the cytokine reference populations.

(B) The distribution of cell adherence on homopolymers. The large shaded area within each outlined rectangle indicates the mean value, and the mean ± 1 SD unit is presented in the narrow columns to the right (plus) and left (minus) of the mean. Data shown are mean values from three different biological replicates (donors) with a minimum of two repeats for each donor (donor 1: four repeats; donor 2: three repeats; donor 3: two repeats).

(C–I) Fluorescent images of cells stained for M1 marker calprotectin (red) and M2 marker mannose receptor (green) and nucleus (DAPI blue) on selected "hit" polymers with either M2 (C and D) or M1 bias (E, F and G). (C) H47: poly(*N*-tris(hydroxymethyl) methyl acrylamide). (D) H37: poly(methacrylamide). (E) H126: poly(isobutyl acrylate). (F) H98: poly(hydroxypropyl acrylate). (G) H24: t-butyl cyclohexyl methacrylate. Examples of (H) highly adhesive H42: poly(cyclohexyl methacrylate), and (I) poorly adhesive H39: poly(tridecafluorooctyl methacrylate). Scale bars, 200 μm.

The highest level of MR expression, an M2 marker, was observed from monocytes seeded on C255 (H88-co-H25), C140 (H94-co-H126), and C186 (H29-co-H126) in Figures 3F–3H. Monocyte polarization toward M2-like was evidenced by 5-fold higher number of M2-like than M1-like cells on these co-polymers. A similar number of M2- and M1-like cells were observed on C398 (H15-co-H113) (Figure 3I) and C408 (H9-co-H117) (Figure 3J); hence, they were considered as M0-like co-polymers. A number of M1 polarizing co-polymers were identified, as evidenced by high levels of calprotectin expression, which resulted in a 10-fold lower M2/M1 ratio: C176 (H125-co-H133) (Figure 3C), C170 (H41-co-H42) (Figure 3D), and C240 (H3-co-H29) (Figure 3E). The highest number of adhered cells were observed on co-polymer C56 (H50-co-H29) (411 ± 143 cells) while C358 (H29-co-H115) had the lowest number of the cells (19 ± 6 cells) (Figures 3K and 3L). Co-polymers C56 (H50-co-H29) (411 ± 143 cells), C386 (H71-co-H126) (363 ± 99 cells), C32 (H25-co-H67) (379 ± 112 cells), C347 (H3-co-H126) (328 ± 126 cells), and C295 (H94-co-H71) (347 ± 166 cells) from the second-generation array had the highest number of attached cells; however, interestingly none of their constituent homopolymers had a significantly high cell attachment, suggesting a synergistic effect upon combination. Co-polymers C358 (H29-co-H115) (18.8 ± 6 cells), C209 (H35-co-H126) (47 ± 22 cells), C434 (H35-co-H123) (51 ± 17 cells), C94 (H35-co-H47) (54 ± 9 cells), and C48 (H50-co-H47) (56 ± 19 cells), on the other hand, had the lowest number of attached cells, consistent with low cell attachment to their constituent homopolymers. Monomer

Please cite this article in press as: Rostam et al., Immune-Instructive Polymers Control Macrophage Phenotype and Modulate the Foreign Body Response *In Vivo*, Matter (2020), https://doi.org/10.1016/j.matt.2020.03.018

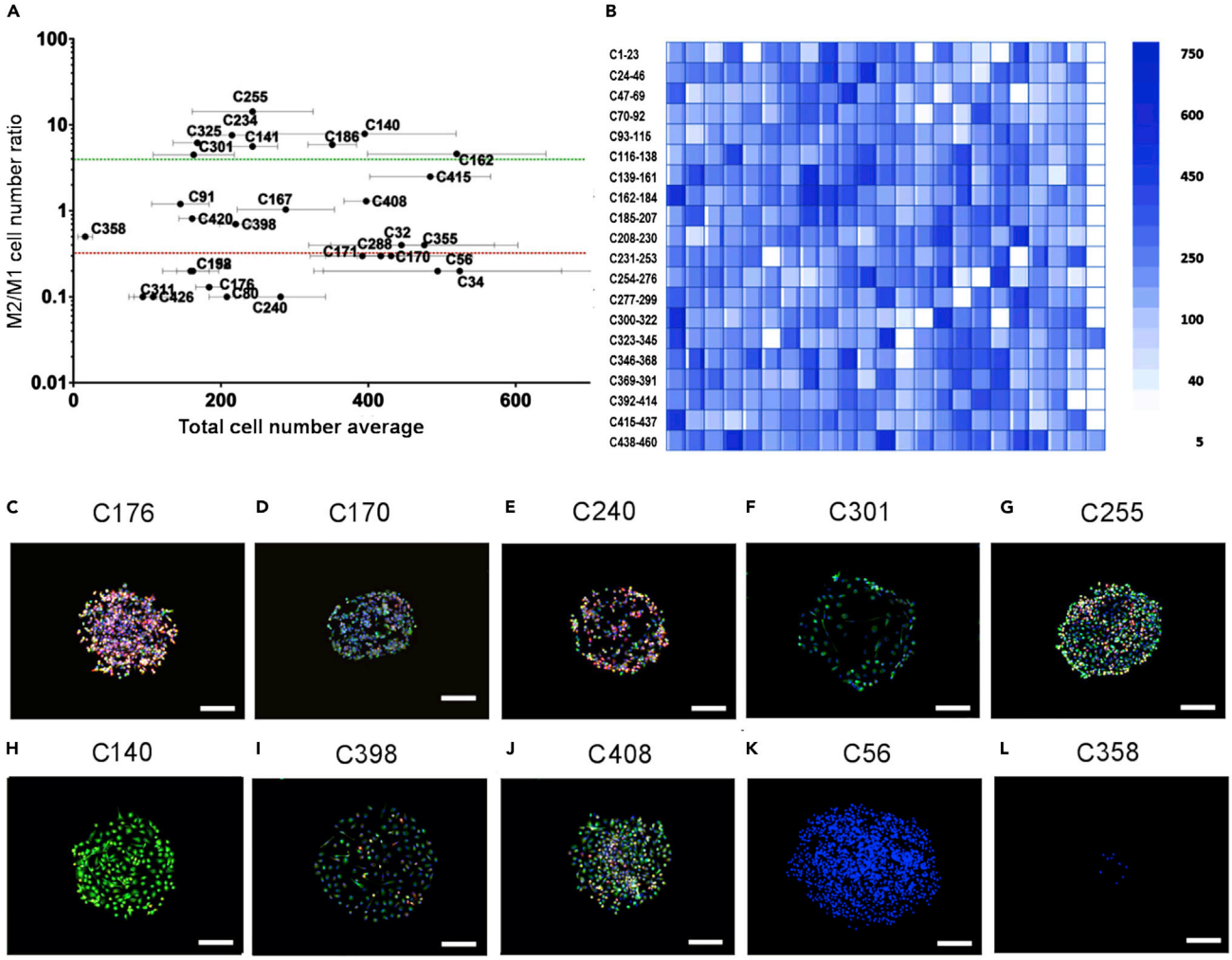

Figure 3. Impact of Co-polymers on Macrophage Polarization and Cell Adherence

(A) Scatterplot showing M2/M1 cell number ratio of macrophages on co-polymers. Data shown are mean values from three different biological replicates (donors) including three technical repeats for each donor. Co-polymers with M2/M1 cell number ratios above the upper green dashed line highlight M2-like co-polymer hits (3.9 ± 0.5) and those below the lower red dashed line (0.3 ± 0.05) show co-polymers that induced M1-like polarization to a greater extent than in the cytokine reference populations.

(B) Average number of adherent cells on co-polymer array. Numbers indicate the co-polymer identity. The large shaded area within each outlined area indicates the mean value, and the mean ± 1 SD unit is presented in the narrow columns to the right (plus) and left (minus) of the mean.

(C–J) Fluorescent images of co-polymers that induce M1 (C–E) and M2 (F–H) bias, or similar number of M1 and M2 bias cells (M0) (I and J). Red shows calprotectin (M1 marker), green mannose receptor (M2 marker), and blue DAPI (nuclear stain).

(K and L) Exemplar co-polymers with high (K) and low (L) cell attachment. Scale bars, 200 μm.

H35: poly(hexyl acrylate) was a constituent of the second, third, and fourth least adherent co-polymers, indicating that this monomer may be involved in preventing cell attachment. Such different cell attachment did not associate with a particular macrophage polarization status. Among the polymers that induced M2-like or M1-like polarization, C162 (H42-co-H126) (M2-like) and C170 (H42-co-H141) (M1-like) (Figure 3D) were the most cell-attractive polymers with 520 ± 2 cells and 431 ± 54 cells, respectively, while C164 (H24-co-H98) (M2-like) and C311 (H24-co-H61) (M1-like) were the least cell-attractive polymers with 125 ± 9 and 94 ± 24 cells attached, respectively (Figure 3B).

Please cite this article in press as: Rostam et al., Immune-Instructive Polymers Control Macrophage Phenotype and Modulate the Foreign Body Response *In Vivo*, Matter (2020), https://doi.org/10.1016/j.matt.2020.03.018

Correlation of Immune-Instructive Behavior with Polymer Chemistry Using Machine Learning

Data generated by high-throughput experiments can be used to develop polymer structure-cell response models using machine learning (see Supplemental Experimental Procedures). These models can enable the prediction of the immune-instructive properties of new materials yet to be synthesized by identification of the types of chemical features that promote or prevent macrophage attachment and polarization.[22–24] To test the applicability of this approach to our dataset, we undertook a computational study to identify important chemical descriptors in macrophage attachment and polarization. As cell attachment and polarization were both equally important, we trained machine-learning models to predict the class of a composite dependent variable, log(M2/M1 ratio) multiplied by the cell attachment. This variable has large positive or negative values for desirable materials with high attachment and polarization (M2 or M1) and low values for those with low attachment and/or low polarization. We generated a two-class predictive model for this parameter by assigning materials with most positive value for the composite variable to the anti-inflammatory phenotype class and the materials with most negative values for the composite variable in the pro-inflammatory class. The anti- and pro-inflammatory classes were defined after clustering the dataset and selecting those instances from the clusters with the highest and lowest values found for the composite variable (see Supplemental Experimental Procedures). To provide chemically informative models, we encoded the various polymer chemistries using molecular signature descriptors that relate directly to polymer structure.[25] We used a LASSO (least absolute shrinkage and selection operator) to eliminate uninformative and less informative descriptors, and generated two-class models using three of the most common machine-learning algorithms, Random Forest, Support Vector Machines, and Multilayer Perceptron.[26–29] All three of these non-linear methods generated models of similar accuracy, as might be expected given that descriptor quality is the most important factor determining model quality. The model with the greatest accuracy assigned the materials to the correct classes with an accuracy of 80% (see Supplemental Experimental Procedures). The molecular features that generated the highest values of the composite variable (log(M2 polarization) × total cell attachment), i.e., that induced the most anti-inflammatory macrophage phenotype with a high cell attachment, are shown in Supplemental Experimental Procedures, which also shows the performance of this model. Alkoxy molecular fragments were found to contribute strongly to the model, with propyloxy, 2,3-dimethylpropyloxy and ethylene glycol fragments appearing at the top of the list. A fluorinated *tert*-butyl and methacrylamide fragment also appeared to have a strong influence on the model, as does a more sterically hindered 2,2,3-trimethylbutyl structure. These observations provide some guidance toward the choice of monomer structure for future rational design of monomers, with the selective combination of branched and alkoxy fragments potentially able to enhance this effect. An implication of this model is that consideration of both steric and electronic factors are important for macrophage response, exemplifying the feasibility of combining high-throughput experiments and machine learning to identify materials chemistry to be a significant driver of immune cell polarization.

Functional Assays Confirm Phenotype Determined by High-Throughput Experiments

To find out whether the changes in cell attachment due directly to the polymer surface marker expression toward M1- or M2-like phenotypes on different polymers were also reflected in cell function, we investigated the cytokine profile and phagocytic ability of macrophages differentiated on a selection of polymer (Figure S2).

Please cite this article in press as: Rostam et al., Immune-Instructive Polymers Control Macrophage Phenotype and Modulate the Foreign Body Response *In Vivo*, Matter (2020), https://doi.org/10.1016/j.matt.2020.03.018

Based on array data and scalability, four polymers were selected that were shown *in vitro* to induce either M1-like (H24 and C170) or M2-like (C255 and C301) phenotypes. These polymers were scaled up to a 24-well format followed by culturing monocytes on polymer-coated plates for 6 days before cytokine quantification. Cells cultured on tissue culture plastic with no polarizing cytokines (naive macrophages) were used as controls. Cells differentiated on H24 produced significantly higher levels of the pro-inflammatory cytokine tumor necrosis factor α (TNF-α) compared with naive macrophages (Figures S2A–S2D). This polymer also induced the production of higher levels of IL-1β, another pro-inflammatory cytokine, but this did not reach statistical significance. Interestingly, C170, the other M1 polarizing polymer, induced higher levels of IL-10 than all other polymers in this assay except for the M2 polarizing polymer C301, which also induced significantly higher levels of IL-10 production. Therefore, cells polarized on H24 (M1-like) and C301 (M2-like) had a cytokine profile in line with their surface phenotypes, and for other M1- and M2-like polarizing polymers we detected a mixed cytokine profile. Our data highlighted the ability of different polymers to drive macrophage polarization toward distinct functional phenotypes that are akin to their cytokine polarized counterparts but not identical. To ensure cell attachment was due to the polymer coating itself and not to cell viability or toxicity, we performed live/dead staining and cytotoxicity tests on the selected lead polymers. Results reveal that the polymer-coated surfaces were consistently non-cytotoxic and cell viability was above 95% following 6-day culture with monocytes (Figure S3). We can therefore conclude that differences in cell attachment on different polymers are due to adherence and not toxicity. The phagocytosis of zymosan particles (a model for recognition of microbes by the innate immune system) by macrophages polarized on C170 (M1 polarizing polymer) was significantly higher than in naive macrophages followed by cells polarized on polymer C301 (M2 polarizing polymer) (Figures S2E–S2M).

Differential Protein Deposition Plays a Role in the Immune-Instructive Capacity of Different Polymers

Following overnight incubation in media, the resultant deposited protein thickness on the polymers was measured by X-ray photoelectron spectroscopy. The protein layer on M1-like polymers (H24 and C170) was found to be 2-fold thicker than the thickness of the protein layer on the naive (C398 and C408) and M2-like polymers (C255 and C301) (Figure S4A), consistent with previous findings.[26] This suggests that it is possible that the total amount of adsorbed protein plays a role in differential polarization of macrophages.

To understand the mechanism behind the differential polarization of macrophages identified within the polymer library, we examined the hypothesis that surface absorbed proteins may influence the macrophage polarization state. Accordingly, we incubated three polymer surfaces that elicited different macrophage polarization in complete culture medium supplemented with fetal bovine serum (FBS) overnight, after which a light wash was used to remove weakly bound material (Figure S5). The more strongly bound species were extracted from the surface using a concentrated urea solution and analyzed by mass spectrometry following the method we have described previously.[30] A total of 137 proteins were detected on the surface of H24 (M1-like), 126 on C301 (M2-like), and 211 on C398 (M0-like) polymers (Figure S4B). One hundred proteins were found to be common to all three polymer surfaces, while 10 were shared only between H24 (M1-like) and C301 (M2-like) (Table S4). There were only five proteins unique to H24 (M1): *Apolipoprotein C-II*, *Dickkopf-like 1*, *Heat-shock protein β1*, *N-acetylglucosamine-1-phosphotransferase subunit γ*, and *Osteomodulin*. Interestingly, *Apolipoprotein C-II* has been reported to

enhance macrophage pro-inflammatory responses including reactive oxygen production and TNF-α expression.[31,32] However, there are mixed reports on the immune-modulatory role of *Dickkopf-like 1*, with some studies showing its role in enhancing inflammatory interactions while others report its ability to suppress inflammatory effects.[33,34] *Heat-shock protein β1* has been shown to stimulate inflammation and pro-inflammatory gene expression.[35,36] However, it has been suggested that the exogenous *Heat-shock protein β1* may also have some anti-inflammatory or immune-regulatory effect on monocytes as evidenced by induction of IL-10 production after stimulation of human monocytes with recombinant human *Heat-shock protein β1*.[37] The proteins uniquely adsorbed on M2-like polymer (C301) were *C-type Lectin Domain Family 11-member A* (*CLEC11A*), *Agglutination Factor XI*, *Rhophilin-2*, and *Transgelin-3*. Little is known about the function of any of these proteins in macrophage polarization except *Agglutination Factor XI*, which has been shown to attenuate inflammation in a mouse model of polymicrobial sepsis.[38] There seemed to be no direct correlation with the number of proteins identified with the surface thickness of protein layer, but some of the uniquely adsorbed proteins on different polymers may play a role in macrophage polarization, which is a point for future studies.

M1 and M2 Polymer Hits Induce Differential Tissue Response as Evidenced by Collagen Deposition and Immune Cell Infiltration

Polymer hits H24, C170 (M1-like), C255, C301 (M2-like), and C398 and C408 (M0-like) were coated onto clinical-grade silicone rubber tube segments using a dip-coating process and implanted subcutaneously into mice for a period of 28 days. Hematoxylin and eosin (H&E) and Masson's trichrome (MTC) stains were used to assess the tissue inflammatory response in terms of inflammatory cell components, angiogenesis, and collagen deposition (Figures 4A and 4B). A typical foreign body response involves rapid and early infiltration of neutrophils, closely followed by macrophages. The intensity of cell infiltration varied between polymers, from an overt cell infiltration in non-coated silicone followed by H24 and C170 (M1-like) polymers, and mild/sparse immune cell infiltration for C398 and C408 (M0-like), to significantly fewer cells for C255 and C301 (M2-like) coatings (Figure 4A). This is consistent with the *in vitro* observations, whereby H24 and C170 elicited a more M1-like phenotype response and C255 and C301 a more anti-inflammatory M2-like response, whereas C398 and C408 were assigned as M0-inducing polymers. It has been shown that as pro-inflammatory macrophages increase, additional neutrophils are recruited.[39] Consistent with this in Figures 4C and 4D, increases in macrophages and neutrophils were detected near the surface of M1-like polymers H24 and C170. Macrophages, especially those of an M2-like phenotype, are involved in tissue repair and remodeling through release of growth factors and cytokines.[39] These promote the recruitment of fibroblasts, which secrete matrix molecules and collagen to bring about tissue repair or excessive extracellular matrix deposition and fibrosis if activated continuously. Collagen deposition at the perilesional tissue using MTC is shown in Figure 4B. Non-coated silicone and C255 showed the thickest collagen layer, along with C301 and H24 (Figure 4E), consistent with the induction of M2-like behavior of the co-polymers C255 and C301 observed *in vitro*. Intriguingly, C398 and C408, the M0-inducing polymers, showed the least amount of collagen deposition. These observations suggest that while sustained and selective M1- or M2-like macrophage activation could lead to brisk inflammation or excessive collagen deposition, respectively, the presence of both M1- and M2-like cell types at similar level (seen in M0 polymers) of foreign body site reduces fibrotic tissue formation. This is in line with evidence from different experimental models of inflammatory tissue injury and fibrosis;[40] however, more *in vivo* studies

Please cite this article in press as: Rostam et al., Immune-Instructive Polymers Control Macrophage Phenotype and Modulate the Foreign Body Response *In Vivo*, Matter (2020), https://doi.org/10.1016/j.matt.2020.03.018

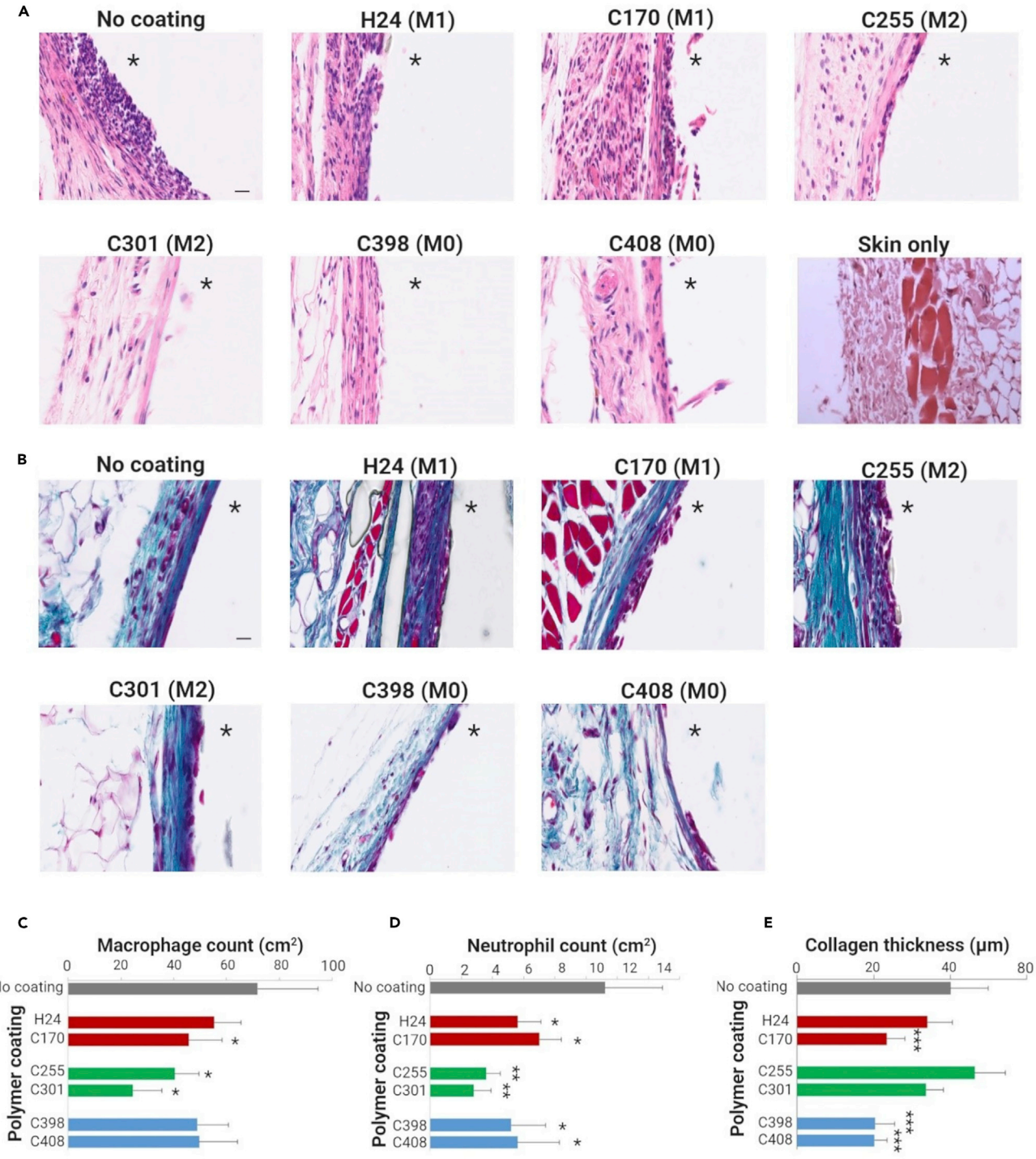

Figure 4. Histological Analysis of Tissue Sections following 28-Day Implantation Polymer-Coated Catheter Segments in a Rodent Model

(A and B) Sections of tissue surrounding the foreign body site (asterisk) were stained with (A) H&E and (B) MTC 4 weeks post implantation. Representative images show H&E and MTC stains with varying extents of foreign body response to each of the polymer coatings (no coating, M1-like [24, 170], M2-like [255, 301], and M0-naïve-like [398, 408] phenotypes from *in vitro* studies) including cell migration, macrophage, neutrophil, and fibroblast infiltration and collagen thickness as a sign of fibrosis.

(C–E) Infiltration counts of (C) macrophages and (D) neutrophils from sites surrounding the foreign body and (E) collagen thickness measured from MTC stains as an indication of fibrosis. All data are presented as the mean ± SD (n = 2 and n = 5). Significance was calculated by one-way ANOVA with Tukey's post hoc analysis: *p < 0.05, **p < 0.01, ***p < 0.001. Scale bar, 25 μm. Figure created with BioRender.

on multiple M1, M2, and M0 polymers would need to take place to confirm these observations.

Characterizing the macrophage phenotype at the catheter-tissue interface was carried out using the pro-inflammatory marker inducible nitric oxide synthase (iNOS) and the anti-inflammatory marker arginase-1 (Arg-1). A double-stain immunofluorescence method was used to stain the tissue sections with cells expressing iNOS labeled in green and cells expressing Arg-1 labeled in red. Representative images of cells exposed to non-coated catheter segments and catheters coated in polymers H24, C170, C255, C301, C398, and C408 are shown in Figures S6A–S6G. Macrophages display a spectrum of activation phenotypes, and the relative proportion of M1 or M2 markers can be used as a handle to determine the type of activation status.[41] Figure S6H shows the ratio of M2/M1 cells in the tissue near the polymer surface. An M2/M1 ratio close to 1.0 was shown by polymer C408 (M0 polymers), where the presence of equal numbers of iNOS or Arg-1 expressing cells seemed to support tissue homeostasis. A more pronounced M1-like phenotype was shown by polymer C170 and a more pronounced M2-like phenotype by polymer C301. These data are broadly in line with the pro- and anti-inflammatory phenotypes observed in *in vitro* high-throughput screening and *in vivo* histological data. Following the rapid high-throughput screening approach to assess the likely effect of multiple polymers on macrophage polarization, future scale-up experiments and *in vivo* studies on lead polymers will focus on assessing multiple pro- and anti-inflammatory markers as well as qRT-PCR to determine the relative mRNA expression of transcription factors to further support the characterization of macrophage phenotype.[17,42]

Conclusions

Our data clearly show that unbiased *in vitro* screening of a large array of polymer chemistries with monocytes successfully identified novel materials with potent immune-modulatory properties, validated in a murine *in vivo* model where pro- or anti-inflammatory responses were shown by histological examination. The polymer structure-cell response relationships could be modeled using machine learning using descriptors of the monomer chemistry, highlighting the potential to undertake "immune-instructive" rational design. Macrophage polarization toward pro- and anti-inflammatory phenotypes was closely linked to the extent of protein deposition on the polymers. Identifying new polymers with immune-modulatory properties and elucidating the molecular mechanisms involved offers exciting possibilities for the rational design of novel bioinstructive materials with numerous clinical applications from implants and vaccine adjuvants to tissue regeneration and drug delivery.

RESOURCE AND DATA AVAILABILITY

This study did not generate new unique reagents. All relevant data are available from the University of Nottingham's Research Data Management Repository https://rdmc.nottingham.ac.uk.

EXPERIMENTAL PROCEDURES

Polymer Array Synthesis

Polymer microarrays were synthesized using methods previously described.[16,43] In brief, polymer microarrays were formed using an XYZ3200 dispensing station (Biodot) and metal pins (946MP6B, Arrayit). The printing conditions were O_2 < 2000 ppm, 25°C, and 35% humidity. To initiate the polymerization, we irradiated arrays with UV (365 nm) for 1 min directly after printing and for a further 10 min at

Please cite this article in press as: Rostam et al., Immune-Instructive Polymers Control Macrophage Phenotype and Modulate the Foreign Body Response *In Vivo*, Matter (2020), https://doi.org/10.1016/j.matt.2020.03.018

the end of the print run. Each polymerization solution was composed of monomer (50% [v/v]) in dimethylformamide with photoinitiator 2,2-dimethoxy-2-phenyl acetophenone (1% [w/v]). Six replicate spots were printed on each slide. Monomers were purchased from Aldrich, Scientific Polymers, and Polysciences and printed onto epoxy-coated slides (Xenopore) dip-coated with poly(2-hydroxyethyl methacrylate) (pHEMA) (4% [w/v], Sigma) in ethanol (95% [v/v] in water). Arrays were sterilized by exposure to UV light for 15 min prior to cell culture. The hits materials were scaled up as polymer coupons formed by pipetting polymerization solution (6 μL) onto a pHEMA-coated slide and irradiating for 10 min at O_2 < 1,300 ppm with a UV source (365 nm). Once formed, volatile components were removed from the polymers at <50 mTorr for 7 days. Polymer wettability was characterized by water contact angle measurements and chemistry was identified by time-of-flight secondary ion mass spectrometry as previously described.[44,45]

Preparation of Polymers Scaled Up into Well Plates

The polymerization solution for the selected hits containing the monomer mixed with photoinitiator (1% [w/v]) was dispensed into 24-well polypropylene plates and polymerized under UV light (365 nm) for 1 h in the presence of argon. Remaining volatile components were removed at <50 mTorr for 72 h. The polymer surfaces were UV sterilized for 20 min and washed with sterile phosphate-buffered saline (PBS) before use. Tissue culture polystyrene was used as a control surface.

Polymerization for Catheter Coating

α,α′-Azoisobutyronitrile (1 wt % to monomer) was added to a solution of degassed monomer (M1-like H24: t-butyl cyclohexyl methacrylate; M1-like C170: cyclohexyl methacrylate/dimethylamino-ethyl methacrylate 2:1; M2-like C255: butoxyethyl methacrylate/dodecafluoro-7-(trifluoromethyl)-octyl acrylate 2:1; M2-like C301: cyclohexyl methacrylate/isodecyl methacrylate 2:1; M0-like C398: ethylene glycol dimethacrylate/heptafluorodecyl methacrylate 2:1; M0-like C408: butoxyethyl methacrylate/dodecafluoro-7-(trifluoromethyl)-octyl acrylate 2:1) (25 wt % in toluene) under argon followed by bis[(difluoroboryl)diphenylglyoximato]cobalt (II) (0.5 wt % to monomer). The reaction mixture was then placed immediately into a preheated +80°C oil bath and stirred for 18 h. The polymer solution was precipitated twice by dropwise addition to stirred hexane at +4°C. The isolated, purified material was then stored under vacuum (<1 mbar) for 48 h before use to remove any remaining volatiles. Gel-permeation chromatography (GPC) of samples was carried out on a Polymer Labs GPC 50 with 2× PLgel Mixed-D columns and *N*,*N*-dimethylformamide containing 0.1 wt % LiBr eluent. GPC calibration was carried out using poly(methyl methacrylate). M1-like H24: M_n = 20,364 g mol^{-1}, M_W = 77,476 g mol^{-1}, PD = 3.80; M1-like C170: M_n = 135,610 g mol^{-1}, M_W = 227,088 g mol^{-1}, PD = 1.67; M2-like C255: M_n = 100,759 g mol^{-1}, M_W = 538,254 g mol^{-1}, PD = 5.34; M2-like C301: M_n = 169,130 g mol^{-1}, M_W = 416,118 g mol^{-1}, PD = 2.46; M0-like C398: M_n = 36,319 g mol^{-1}, M_W = 341,799 g mol^{-1}, PD = 9.41; M0-like C408: M_n = 417,663 g mol^{-1}, M_W = 1,347 357 g mol^{-1}, PD = 3.22.

Preparation of Polymer-Coated Catheters

Silicone catheters (Smith medical 8 Foley catheter) were cut into 15 × 1-cm-length sections and activated using oxygen plasma (50 W, 13.56 MHz, 1 min, 1.0 mbar O_2). These were immediately attached to a 21-gauge needle by piercing the catheter wall with the needle and dipped by hand into NuSil MED-163 silicone primer before being allowed to dry under ambient conditions for 30 min. The silanized catheters were next dip-coated three times by hand into 3% (v/v) polymer in toluene

solutions, leaving 30 min drying time between dips. After completion of the dip-coating process, they were placed under vacuum (<0.3 mbar) for 1 week prior to use.

Monocyte Isolation and Culture

Buffy coats were obtained from healthy donors (National Blood Service, Sheffield, UK) after obtaining informed written consent and following ethics committee approval (Research Ethics Committee, Faculty of Medicine and Health Sciences, University of Nottingham). Monocytes were isolated from peripheral blood mononuclear cells. A MACS magnetic cell separation system (CD14 MicroBeads positive selection with LS columns, Miltenyi Biotec) was used for the isolation as previously described.[46,47] The purity of monocytes by this method was about 95% as determined by CD14 expression using flow-cytometric analysis. Isolated monocytes were prepared to a cell density of 1×10^6 cells/mL in RPMI-1640 medium (10% FBS, 100 μg/mL streptomycin, 2 mM L-glutamine, and 100 U/mL penicillin [Sigma-Aldrich]). For screening, 15 mL of the suspension (15×10^6 monocytes) were seeded on microarray surfaces and incubated (37°C, 5% CO_2) in a humidified incubator for 6 days.

Immunostaining of Macrophages on Polymer Arrays

On day 6, all adherent cells on polymer arrays were fixed in paraformaldehyde (4%) (EMS Diasum) in PBS, then blocked with bovine serum albumin (BSA) (3%, Sigma-Aldrich) and glycine (1%, Fisher Scientific) in PBS. Subsequently, another blocking step was carried out using goat serum (5%, Sigma) in PBS. Adherent cells were stained with anti-human calprotectin mouse immunoglobulin G1 (IgG1) antibody (2 μg/mL) (Thermo Scientific), and rabbit CD206 (MR) anti-human primary antibody (1 μg/mL) (Abcam) followed by 1 h of incubation at room temperature. After washing, cells were stained with Rhodamine-x goat anti-mouse IgG (H + L) secondary antibody (8 μg/mL, Invitrogen), and Alexa Fluor-488 goat anti-rabbit IgG (H + L) secondary antibody (8 μg/mL Invitrogen) for another hour at room temperature. In all samples the nuclei were stained with 4′,6-diamidino-2-phenylindole (DAPI) (250 ng/mL, Invitrogen) for 5 min at room temperature. Slides were covered with FluorSave anti-fade medium (Calbiochem) and mounted with Fluoromount (Sigma-Aldrich). Arrays were imaged using an Olympus IX51 fluorescence microscope and a Smart Imaging System (IMSTAR). Images were analyzed using CellProfiler cell image analysis software (http://www.cellprofiler.org/) to identify the number of positively MR and calprotectin-stained cells from four array replicates. To assess polymer induction of macrophage polarization, we first established reference fluorescence measurements for the expression of these markers in populations of cytokine polarized M1 (IFN-γ 20 ng/mL + GM-CSF 50 ng/mL) or cytokine polarized M2 macrophages (IL-4 20 ng/mL + M-CSF 50 ng/mL) cultured on glass slides. Fluorescence images of a minimum of 100 cells in 9 fields of view were analyzed for each cytokine polarization in two different experiments for the same biological replicate (cell donor) prepared on the same day. The expression levels of calprotectin and MR in cytokine polarized M1 and M2 macrophages (generated as we have previously described) were used for setting the thresholds when analyzing macrophage polarization on the polymer arrays.[17] The maximum calprotectin fluorescent pixel intensity for each cell was used to represent its fluorescence expression, and the average value was calculated for each cytokine polarized cell to represent the mean cellular expression for M1 polarized cells. The same procedure was followed for the MR fluorescence to obtain a mean cellular fluorescence expression for cytokine polarized M2 cells. Mean threshold fluorescence values for calprotectin and MR expression for cytokine polarized M1 or M2 cells were used to categorize the phenotype of the individual macrophage cells when they exceeded these levels of

fluorescence values. The cell populations polarized by cytokines to M1 and M2 were determined to have an M2/M1 cell number ratio of M2 = 3.8 ± 0.6 and M1 = 0.4 ± 0.05, respectively in donors for the homopolymer (first-generation) experiments. This was slightly different from donors used for the co-polymer (second-generation) experiments in which the ratio was 3.9 ± 0.5 and 0.3 ± 0.05 for M2 and M1 conditions, respectively (Figure S1). This is due to inter-individual variation between donors. For macrophages on polymer microarrays, cell populations with M2/M1 cell number ratios below or above those found in these reference populations were considered to represent polymers inducing predominantly M1 or M2 differentiation, respectively.

Cytokine Quantification Assay

The level of TNF-α, IL-1β, CCL18, and IL-10 secreted into the media by macrophages cultured on scaled-up polymers for 6 days was quantified by sandwich ELISA using DuoSet ELISA development kits (R&D Systems) as per manufacturer's instructions. Culture supernatant was replaced on days 1 (to remove any non-adherent cells) and 3 (to feed the cells) prior to cytokine quantification on day 6.

Phagocytosis Assay

Monocytes were cultured in polymer-coated tissue culture plates for 6 days to allow differentiation to macrophages without cytokine stimulation. This was followed by addition of Alexa Fluor-488-labeled zymosan A (*Saccharomyces cerevisiae*) bioparticles (Thermo Fisher Scientific) (≈25 particles/cell). Following an incubation period of 30 min (at 37°C, 5% CO_2), cells were washed with sterile PBS (five times) to remove unphagocytosed particles. Tissue culture plastic was used as a control surface. Cells were then imaged with a Zeiss LSM 880 confocal microscope using a 40× oil objective lens (numerical aperture = 1.30), a 488-nm argon laser, and 500- to 535-nm emission bandwidth. Images were captured using Zen digital imaging software.

Cell Viability and Cytotoxicity Assay

Monocytes were cultured on M1-like (H24, C170), M2-like (C255, C301), and M0-like (C398) polymers. On day 6, supernatants were collected and cytotoxicity was assessed using a Toxilight bioassay kit as per manufacturer's instructions (Lonza Bioscience). A live/dead stain (Thermo Fisher Scientific) was also performed on the cells on each of the polymer surfaces following 6 days of culture to assess viability. Experiments were carried out in triplicate using three different donors. Live controls consisted of cells cultured on a tissue culture plastic surface. For dead control, cells on tissue culture plastic surfaces were treated with Triton X-100.

Proteomic Analysis of the Adsorbate Layer on Hit Polymers

X-Ray Photoelectron Spectroscopy Analysis of Protein Layer on Hit Polymers

M1-like (H24, C170), M2-like (C255, C301), and non-polarizing (C398, C408) polymers were printed in a microarray format as described earlier. The polymer array was immersed in RPMI-1640 medium (3 mL) (supplemented with 10% FBS, 1% L-glutamine, 1% penicillin-streptomycin), in 4-well plates and incubated overnight (~24 h at 37°C, 5% CO_2). After incubation, the arrays were gently washed in ultrapure water (10 mL) for 10 min. The process was repeated ten times, after which the samples were vacuum dried for ≥3 days prior to measurement. The protein adsorbate on each polymer spots was assessed at Kratos Analytical (Manchester, UK) with a Kratos AXIS Nova X-ray Photoelectron Spectrometer equipped with dual Al/Ag monochromated X-ray source. The protein thickness was calculated from quantification of the nitrogen contribution using a method previously outlined.[48]

Please cite this article in press as: Rostam et al., Immune-Instructive Polymers Control Macrophage Phenotype and Modulate the Foreign Body Response *In Vivo*, Matter (2020), https://doi.org/10.1016/j.matt.2020.03.018

Protein Extraction

Tissue culture 4-well polystyrene plates (Nalge Nunc International, USA) were activated using O_2 plasma (0.09 mbar, 50 W) for 10 min, then coated with a selection of M1, M2, or non-polarizing (polymers H24, C301 and C398, respectively) monomer solutions (50% [v/v] monomer and 1% [w/v] photoinitiator, 2,2-dimethoxy-2-phenylacetophenone in isopropyl alcohol) at the required ratio. UV polymerization was conducted for 45 min under an Ar-filled atmosphere (O_2 < 2000 ppm). The polymer-coated 4-well polystyrene plates were kept under vacuum for ≥7 days prior to use. Supplemented medium used for cell culture (5 mL) was added to each polymer-coated well, and the 4-well plates were incubated overnight (~24 h) at 37°C and 5% CO_2. The extraction of surface-adsorbed proteins was based on the Hammad et al.[30] protocol with slight modifications. The medium was aspirated and the polymer surfaces were rinsed gently with PBS (1 mL) per well for 2 min, then ultrapure water (1 mL) per well for another 2 min, on a reciprocal shaker (75 rpm). An extraction solution made of sodium chloride (1 M), urea (6 M), Triton X-100 (1%), and isopropyl alcohol (50%) was used to extract the surface-adsorbed proteins. To each well, extraction solution (200 μL) was added, and the 4-well plates were incubated on a platform shaker (10–15 rpm) for 1 h at room temperature. The extraction solution was then aspirated into Eppendorf tubes (1.5 mL), and acetone precipitation was conducted using 4× volume cold acetone (−20°C) and incubated for 1 h at −20°C. The samples were centrifuged (13,000 × *g* for 10 min at 4°C) and acetone removed thereafter. The resulting pellets were resuspended in ultrapure water (10 μL) and pooled (per polymer) for protein analysis. The protein concentration was estimated using the Pierce BCA Protein Assay (Thermo Scientific, USA) using BSA as the protein standard. The extracted proteins were also subjected to SDS-PAGE analysis on 4-polyacrylamide gels (15%) for 1 h at 100 V. The gels were stained with Coomassie brilliant blue G-250 or the Pierce Silver Stain kit (Thermo Scientific).

Liquid Chromatography-Tandem Mass Spectrometry Analysis

The extracted surface absorbed proteins (three technical replicates for each polymer) were further examined by liquid chromatography-tandem mass spectrometry (LC-MS/MS) analysis. Protein solutions were subjected to reduction (with dithiothreitol) and alkylation (with iodoacetamide) prior to overnight digestion with trypsin (Promega, USA). All LC-MS/MS experiments were performed using a Dionex Ultimate 3000 RSLC nanoUPLC system (Thermo Fisher Scientific, USA) and a Q Exactive Orbitrap mass spectrometer (Thermo Fisher Scientific). Separation of tryptic digested peptides was performed by a reverse-phase nano Easy-spray column (PepMap C18, 50 mm length × 75 μm internal diameter [i.d.], 100 Å pore size, 2 μm particle size; Thermo Fisher Scientific). Peptides were loaded onto a pre-column (PepMap 100 C18, 5 mm length × 300 μm i.d., 100 Å pore size, 5 μm particle size; Thermo Fisher Scientific) from an Ultimate 3000 autosampler with water and formic acid (0.1%) for 3 min under flow (10 μL/min). After this period, the column valve was switched to allow elution of peptides from the pre-column onto the analytical column. Solvent A was water + formic acid (0.1%) and solvent B was acetonitrile/H_2O (80:20) + formic acid (0.1%). The linear gradient employed was 4%–40% B in 100 min (the total run time including column washing and re-equilibration was 120 min). All *m/z* values of eluting ions were measured in an Orbitrap mass analyzer, set at a resolution of 70,000, and scanned between *m/z* 380 and 1,500. Data-dependent scans (top 20) were employed to automatically isolate and generate fragment ions by higher-energy collisional dissociation (HCD) with normalized collision energy of 32.5% in the HCD collision cell, and measurement of the resulting fragment ions was performed in the Orbitrap analyzer set at a resolution of 35,000. Singly charged

ions and ions with unassigned charge states were excluded from being selected for MS/MS, and a dynamic exclusion of 60 s was employed. Post run, the data were processed using Protein Discoverer version 2.1 (Thermo Fisher Scientific). In brief, all MS/MS data were converted to .mgf files, and the files were then submitted to the Mascot search algorithm (Matrix Science, UK) and searched against the Uniprot bovine database (BosTaurus_20170607, 24,148 sequences; 12,824,305 residues) and common contaminant sequences (115 sequences, 38,274 residues). Variable modifications of oxidation, deamidation, and carbamidomethyl were applied. The peptide and fragment mass tolerances were set to 5 ppm and 0.1 Da, respectively. A significance threshold value of $p < 0.05$ and a peptide cutoff score of 20 were also applied. The lists of proteins for each hit polymer were then compared manually, and unique proteins were identified based on the presence in minimum two of the three technical replicates for each polymer.

In Vivo Murine Model

Sections of medical-grade silicone urinary catheter tube (2.7 × 5-mm Smith medical 8 Foley catheter) were cut longitudinally in half and served as a model implant. M1 (H24, C170), M2 (C301, C255), and non-polarizing (C398, C408) polymers were manually dip-coated onto the silicone tube segments using NuSil MED-163 silicone primer and allowed to dry under ambient conditions for 30 min. They were then manually dip-coated three times in a solution of each of the polymers (1 wt %) in toluene, leaving 30 min drying time between dips. Coated segments were placed under vacuum (<0.3 mbar) for 1 week prior to use. Catheter sections without a polymer coating served as controls. Sterilization consisted of exposure to UV light for a period of 20 min. All *in vivo* studies were approved by the University of Nottingham Animal Welfare and Ethical Review Board and were carried out in accordance with Home Office authorization under project license number 30/3238. Age-matched adult female BALB/c mice (Charles River) were housed in individually ventilated cages under a 12-h light cycle with food and water *ad libitum*. 1 h before catheter implantation, analgesia (carprofen) was administered subcutaneously (2.5 mg/kg), animals where anesthetized and hair removed by shaving, and the area was sterilized with Hydrex (Ecoblab). A small incision was made in the flank, and individual catheter segments were loaded into a trocar needle (9 g) and injected subcutaneously on one side of the mouse, the other side serving as a sham. The wound was sealed using Gluture skin glue. All mice were monitored until they recovered from anesthesia, and inflammation at the site of implantation, behavioral changes, and other adverse reactions were monitored throughout the duration of the experiment. At the end of the experiment, on day 28, mice were humanely sacrificed by CO_2 euthanasia.

Histological Analysis

The catheter segment and surrounding skin was excised and placed in zinc fixative for 24 h. Following fixation, the tissue was loaded into cassettes and placed onto a Leica TP1020 tissue processor for dehydration through a series of ethanol solutions followed by incubation in xylene. Tissue was then embedded in paraffin wax and sliced into sections (7 μm) using a Leica RM2245 microtome before mounting onto polylysine-coated slides (Thermo Fisher Scientific). The foreign body response to the polymer coatings was assessed by staining with H&E and MTC. Samples were observed using a Ventana DP200 (Roche) slide scanner with a 40× objective. The histological interpretation of the tissue sections was performed by four of the authors, including two specialized histopathologists.

Phenotype Analysis

Antigen retrieval was carried out by heating tissue sections to 100°C for 20 min in citrate buffer (pH 6). Following washing in deionized water, cells were permeabilized using Triton X-100 (0.1%) for 10 min and rinsed 3 × 5 min in PBS-Tween 20 (0.2%). Non-specific binding was blocked by incubating tissue sections in BSA (5%) with donkey serum (5%) for 1 h at room temperature. Sequential antibody staining was undertaken using goat anti-mouse Arg-1 (1:50; PA5-18392, Thermo Fisher Scientific) and rabbit anti-mouse iNOS (1:50; ab15323, Abcam) antibodies at 4°C overnight. Secondary antibodies, donkey anti-goat IgG (H + L), and donkey anti-rabbit IgG (H + L) labeled with Alexa Fluor-594 and -488 (1:200; A11058 and A21206, Thermo Fisher Scientific), respectively, were applied for 1 h at room temperature to visualize the macrophage cells. Isotype controls and no primary antibody served as controls and showed little background autofluorescence. Images were acquired on a Zeiss LSM880C confocal microscope, and any background fluorescence was subtracted using ImageJ. The mean raw-intensity density of the region of interest around the foreign body site was used to measure the sum of all pixels in the given area. All *in vivo* studies were carried out in duplicate on two separate occasions, and at least five different fields of view were randomly examined in each tissue section. Polymer coatings were blinded to the researchers and revealed at the end of the experiment.

Statistical Analysis

Statistical significance was calculated using one-way ANOVA and Tukey's post hoc analysis, whereby $p \leq 0.05$ was considered as being statistically significant for cytokine, protein thickness, and morphological/phenotypical characteristics of macrophages *in vitro* and *in vivo*. To account for intra-experimental variations between polymer replicates on each array, we used a signal-to-noise ratio (SNR) of 2 as a threshold for detection when evaluating fluorescence intensity, cell adherence, and changes in cell morphology. The SNR was calculated using the ratio of the mean value of the signal and the standard deviation of the noise.

SUPPLEMENTAL INFORMATION

Supplemental Information can be found online at https://doi.org/10.1016/j.matt.2020.03.018.

ACKNOWLEDGMENTS

This project was supported by The EPSRC Program grant in Next Generation Biomaterials Discovery (EP/N006615/1) and a Confidence in Concept Medical Research Council grant. The Cambridge Center for Proteomics is acknowledged for the LC-MS/MS service analysis of surface-extracted proteins. Ian Ward, Denise McLean, and Christopher Gell from the School of Life Sciences Imaging team at the University of Nottingham are acknowledged for assistance in histology and imaging and Declan Sculthorpe from the School of Medicine for aid in whole-slide scanning. A.L.H. acknowledges the University of Nottingham for funding his Nottingham Research Fellowship. H.M.R. acknowledges a Human Capacity Development Program PhD scholarship (Kurdistan Regional Government). A.M.G. acknowledges funding from the European Union's Horizon 2020 research and innovation program under grant agreement 760921 (PANBioRA).

AUTHOR CONTRIBUTIONS

A.M.G., M.R.A., J.C.L., and A.L.H. designed the studies and helped write the paper. H.M.R., L.E.F., L.B., J.C.L., C.M., A.C.K.T., A.L., L.K., M.D., K.L., and D.B. conducted

the experiments. G.P.F. carried out statistical analysis and prepared displays communicating the data with the support of D.A.W., S.E., and M.I. aided the histological interpretation. A.M.G. and M.R.A. conceived and supervised the study.

DECLARATION OF INTERESTS

The authors declare no competing interests. Polymers described in this study are subject to patent application GB2002011.1 (Chemical & Microtopography Effects) (patent pending).

Received: November 21, 2019
Revised: January 29, 2020
Accepted: March 23, 2020
Published: May 1, 2020

REFERENCES

1. Anderson, J.M., Rodriguez, A., and Chang, D.T. (2008). Foreign body reaction to biomaterials. Semin. Immunol. *20*, 86–100.
2. Grainger, D.W. (2013). All charged up about implanted biomaterials. Nat. Biotechnol. *31*, 507–509.
3. Vegas, A.J., Veiseh, O., Doloff, J.C., Ma, M., Tam, H.H., Bratlie, K., Li, J., Bader, A.R., Langan, E., Olejnik, K., et al. (2016). Combinatorial hydrogel library enables identification of materials that mitigate the foreign body response in primates. Nat. Biotechnol. *34*, 345–352.
4. Higgins, D.M., Basaraba, R.J., Hohnbaum, A.C., Lee, E.J., Grainger, D.W., and Gonzalez-Juarrero, M. (2009). Localized immunosuppressive environment in the foreign body response to implanted biomaterials. Am. J. Pathol. *175*, 161–170.
5. Veiseh, O., Doloff, J.C., Ma, M., Vegas, A.J., Tam, H.H., Bader, A.R., Li, J., Langan, E., Wyckoff, J., Loo, W.S., et al. (2015). Size- and shape-dependent foreign body immune response to materials implanted in rodents and non-human primates. Nat. Mater. *14*, 643–651.
6. Biswas, S.K., and Mantovani, A. (2010). Macrophage plasticity and interaction with lymphocyte subsets: cancer as a paradigm. Nat. Immunol. *11*, 889–896.
7. Price, J.V., and Vance, R.E. (2014). The macrophage paradox. Immunity *41*, 685–693.
8. Xue, J., Schmidt, S.V., Sander, J., Draffehn, A., Krebs, W., Quester, I., De Nardo, D., Gohel, T.D., Emde, M., Schmidleithner, L., et al. (2014). Transcriptome-based network analysis reveals a spectrum model of human macrophage activation. Immunity *40*, 274–288.
9. Visan, I. (2016). Macrophage core program. Nat. Immunol. *17*, 1141.
10. Vishwakarma, A., Bhise, N.S., Evangelista, M.B., Rouwkema, J., Dokmeci, M.R., Ghaemmaghami, A.M., Vrana, N.E., and Khademhosseini, A. (2016). Engineering immunomodulatory biomaterials to tune the inflammatory response. Trends Biotechnol. *34*, 470–482.
11. Rostam, H.M., Singh, S., Vrana, N.E., Alexander, M.R., and Ghaemmaghami, A.M. (2015). Impact of surface chemistry and topography on the function of antigen presenting cells. Biomater. Sci. *3*, 424–441.
12. Celiz, A.D., Smith, J.G.W., Patel, A.K., Hook, A.L., Rajamohan, D., George, V.T., Flatt, L., Patel, M.J., Epa, V.C., Singh, T., et al. (2015). Discovery of a novel polymer for human pluripotent stem cell expansion and multilineage differentiation. Adv. Mater. *27*, 4006–4012.
13. Celiz, A.D., Smith, J.G.W., Langer, R., Anderson, D.G., Winkler, D.A., Barrett, D.A., Davies, M.C., Young, L.E., Denning, C., and Alexander, M.R. (2014). Materials for stem cell factories of the future. Nat. Mater. *13*, 570–579.
14. Patel, A.K., Celiz, A.D., Rajamohan, D., Anderson, D.G., Langer, R., Davies, M.C., Alexander, M.R., and Denning, C. (2015). A defined synthetic substrate for serum-free culture of human stem cell derived cardiomyocytes with improved functional maturity identified using combinatorial materials microarrays. Biomaterials *61*, 257–265.
15. Venkateswaran, S., Wu, M., Gwynne, P.J., Hardman, A., Lilienkampf, A., Pernagallo, S., Blakely, G., Swann, D.G., Gallagher, M.P., and Bradley, M. (2014). Bacteria repelling poly(methylmethacrylate-co-dimethylacrylamide) coatings for biomedical devices. J. Mater. Chem. B *2*, 6723–6729.
16. Hook, A.L., Chang, C.-Y., Yang, J., Luckett, J., Cockayne, A., Atkinson, S., Mei, Y., Bayston, R., Irvine, D.J., Langer, R., et al. (2012). Combinatorial discovery of polymers resistant to bacterial attachment. Nat. Biotechnol. *30*, 868.
17. Rostam, H.M., Reynolds, P.M., Alexander, M.R., Gadegaard, N., and Ghaemmaghami, A.M. (2017). Image based machine learning for identification of macrophage subsets. Sci. Rep. *7*, 3521.
18. Rostam, H.M., Singh, S., Salazar, F., Magennis, P., Hook, A., Singh, T., Vrana, N.E., Alexander, M.R., and Ghaemmaghami, A.M. (2016). The impact of surface chemistry modification on macrophage polarisation. Immunobiology *221*, 1237–1246.
19. Safi, W., Kuehnl, A., Nüssler, A., Eckstein, H.-H., and Pelisek, J. (2016). Differentiation of human CD14$^+$ monocytes: an experimental investigation of the optimal culture medium and evidence of a lack of differentiation along the endothelial line. Exp. Mol. Med. *48*, e227.
20. Murray, P.J., Allen, J.E., Biswas, S.K., Fisher, E.A., Gilroy, D.W., Goerdt, S., Gordon, S., Hamilton, J.A., Ivashkiv, L.B., Lawrence, T., et al. (2014). Macrophage activation and polarization: nomenclature and experimental guidelines. Immunity *41*, 14–20.
21. Klinder, A., Markhoff, J., Jonitz-Heincke, A., Sterna, P., Salamon, A., and Bader, R. (2019). Comparison of different cell culture plates for the enrichment of non-adherent human mononuclear cells. Exp. Ther. Med. *17*, 2004–2012.
22. Le, T., Epa, V.C., Burden, F.R., and Winkler, D.A. (2012). Quantitative structure-property relationship modeling of diverse materials properties. Chem. Rev. *112*, 2889–2919.
23. Le, T.C., Penna, M., Winkler, D.A., and Yarovsky, I. (2019). Quantitative design rules for protein-resistant surface coatings using machine learning. Sci. Rep. *9*, 265.
24. Mikulskis, P., Hook, A., Dundas, A.A., Irvine, D., Sanni, O., Anderson, D., Langer, R., Alexander, M.R., Williams, P., and Winkler, D.A. (2018). Prediction of broad-spectrum pathogen attachment to coating materials for biomedical devices. ACS Appl. Mater. Interfaces *10*, 139–149.
25. Churchwell, C.J., Rintoul, M.D., Martin, S., Visco, D.P., Kotu, A., Larson, R.S., Sillerud, L.O., Brown, D.C., and Faulon, J.L. (2004). The signature molecular descriptor - 3. Inverse-quantitative structure-activity relationship of ICAM-1 inhibitory peptides. J. Mol. Graphics Model. *22*, 263–273.
26. Breiman, L. (2001). Random forests. Machine Learn. *45*, 5–32.
27. Cortes, C., and Vapnik, V. (1995). Support-vector networks. Machine Learn. *20*, 273–297.
28. Rosenblatt, F. (1961). Principles of Neurodynamics: Perceptrons and the Theory of Brain Mechanisms (Spartan Books).

29. Rumelhart, D.E., Hinton, G.E., and Williams, R.J. (1986). Learning internal representations by error propagation. In Parallel Distributed Processing: Explorations in the Microstructure of Cognition, *1*, D.E. Rumelhart and J.L. McClelland, eds., Parallel Distributed Processing: Explorations in the Microstructure of Cognition (MIT Press), pp. 318–362.

30. Hammad, M., Rao, W., Smith, J.G.W., Anderson, D.G., Langer, R., Young, L.E., Barrett, D.A., Davies, M.C., Denning, C., and Alexander, M.R. (2016). Identification of polymer surface adsorbed proteins implicated in pluripotent human embryonic stem cell expansion. Biomater. Sci. *4*, 1381–1391.

31. Medeiros, L.A., Khan, T., El Khoury, J.B., Pham, C.L., Hatters, D.M., Howlett, G.J., Lopez, R., O'Brien, K.D., and Moore, K.J. (2004). Fibrillar amyloid protein present in atheroma activates CD36 signal transduction. J. Biol. Chem. *279*, 10643–10648.

32. Wong, Y.Q., Binger, K.J., Howlett, G.J., and Griffin, M.D. (2010). Methionine oxidation induces amyloid fibril formation by full-length apolipoprotein A-I. Proc. Natl. Acad. Sci. U S A *107*, 1977–1982.

33. Ueland, T., Otterdal, K., Lekva, T., Halvorsen, B., Gabrielsen, A., Sandberg, W.J., Paulsson-Berne, G., Pedersen, T.M., Folkersen, L., Gullestad, L., et al. (2009). Dickkopf-1 enhances inflammatory interaction between platelets and endothelial cells and shows increased expression in atherosclerosis. Arterioscler. Thromb. Vasc. Biol. *29*, 1228–1234.

34. Jang, J., Jung, Y., Kim, Y., Jho, E.-H., and Yoon, Y. (2017). LPS-induced inflammatory response is suppressed by Wnt inhibitors, Dickkopf-1 and LGK974. Sci. Rep. *7*, 41612.

35. Alford, K.A., Glennie, S., Turrell, B.R., Rawlinson, L., Saklatvala, J., and Dean, J.L. (2007). Heat shock protein 27 functions in inflammatory gene expression and transforming growth factor-beta-activated kinase-1 (TAK1)-mediated signaling. J. Biol. Chem. *282*, 6232–6241.

36. Henstridge, D.C., Whitham, M., and Febbraio, M.A. (2014). Chaperoning to the metabolic party: the emerging therapeutic role of heat-shock proteins in obesity and type 2 diabetes. Mol. Metab. *3*, 781–793.

37. Vanderbyl, S., MacDonald, N., and de Jong, G. (2001). A flow cytometry technique for measuring chromosome-mediated gene transfer. Cytometry *44*, 100–105.

38. Tucker, E.I., Verbout, N.G., Leung, P.Y., Hurst, S., McCarty, O.J., Gailani, D., and Gruber, A. (2012). Inhibition of factor XI activation attenuates inflammation and coagulopathy while improving the survival of mouse polymicrobial sepsis. Blood *119*, 4762–4768.

39. Butterfield, T.A., Best, T.M., and Merrick, M.A. (2006). The dual roles of neutrophils and macrophages in inflammation: a critical balance between tissue damage and repair. J. Athl. Train *41*, 457–465.

40. Wynn, T.A., and Vannella, K.M. (2016). Macrophages in tissue repair, regeneration, and fibrosis. Immunity *44*, 450–462.

41. Thomas, A.C., and Mattila, J.T. (2014). "Of mice and men": arginine metabolism in macrophages. Front. Immunol. *5*, 479.

42. Zhang, L., Cao, Z., Bai, T., Carr, L., Ella-Menye, J.R., Irvin, C., Ratner, B.D., and Jiang, S. (2013). Zwitterionic hydrogels implanted in mice resist the foreign-body reaction. Nat. Biotechnol. *31*, 553–556.

43. Anderson, D.G., Levenberg, S., and Langer, R. (2004). Nanoliter-scale synthesis of arrayed biomaterials and application to human embryonic stem cells. Nat. Biotechnol. *22*, 863–866.

44. Taylor, M., Urquhart, A.J., Zelzer, M., Davies, M.C., and Alexander, M.R. (2007). Picoliter water contact angle measurement on polymers. Langmuir *23*, 6875–6878.

45. Hook, A.L., and Scurr, D.J. (2016). ToF-SIMS analysis of a polymer microarray composed of poly(meth)acrylates with C6 derivative pendant groups. Surf. Interface Anal. *48*, 226–236.

46. Garcia-Nieto, S., Johal, R.K., Shakesheff, K.M., Emara, M., Royer, P.J., Chau, D.Y., Shakib, F., and Ghaemmaghami, A.M. (2010). Laminin and fibronectin treatment leads to generation of dendritic cells with superior endocytic capacity. PLoS One *5*, e10123.

47. Salazar, F., Hall, L., Negm, O.H., Awuah, D., Tighe, P.J., Shakib, F., and Ghaemmaghami, A.M. (2016). The mannose receptor negatively modulates the Toll-like receptor 4-aryl hydrocarbon receptor-indoleamine 2,3-dioxygenase axis in dendritic cells affecting T helper cell polarization. J. Allergy Clin. Immunol. *137*, 1841–1851.e2.

48. Ray, S., and Shard, A.G. (2011). Quantitative analysis of adsorbed proteins by X-ray photoelectron spectroscopy. Anal. Chem. *83*, 8659–8666.